1 Comparing EM27/SUN observations and TCCON

Observations in Fairbanks began with the Arctic Mobile Infrared Greenhouse Gas Observations (AMIGGO) campaign during 4 August to 15 October 2016, including 20 days of side-by-side observations collected with two EM27/SUN spectrometers, the KIT EM27 and the LANL EM27 (the LANL EM27 is owned by Los Alamos National Laboratories and the KIT EM27 is owned by the Karlsruhe Institute of Technology). Throughout this period the spectrometers exhibited a stable correlation with an average offset of 0.06% (∼0.24 ppm) (see Fig. S1 panel (a)). The LANL EM27 was then operated alongside the Caltech TCCON instrument (Wennberg et al., 2017) in December 2017 (see correlation in Fig. S1 panel (c)), and in September 2018 (see correlation in Fig. S1 panel (d)). Both the LANL EM27 and the KIT EM27 were serviced and upgraded to include dual detectors (allowing for retrievals of X_{CO}; Hase et al. (2016)) in winter 2017/18, and this resulted in an observed reduction in the offset between the two EM27/SUN spectrometers (seen when comparing panels (a) and (b) of Fig. S1). The instrument upgrades in early 2018 also resulted in a reduced offset between the LANL EM27 and Caltech TCCON relative to observations in December 2017 (see Fig. S1 panel (c)). Additional days of side-by-side observations between the KIT EM27 and LANL EM27, after instrument upgrades, were conducted in May, June, and August of 2018, and these also exhibit a stable correlation with a negligible average offset of 0.01% (∼0.04 ppm).

1.1 EM27/SUN ILS measurements

To ensure continued instrument performance, the instrument line shapes (ILS) of each of the two EM27/SUN FTS used in Fairbanks were characterized at multiple times from August 2016 to present using the LINEFIT algorithm (Hase et al., 1999) with methods discussed by Frey et al. (2015) and Hedelius et al. (2016). In previous studies with the EM27/SUN, such as Frey et al. (2019) and Butz et al. (2017) EM27/SUN retrievals are attained with the PROFFIT retrieval algorithm (Hase et al., 2004), which requires an empirical input of the non-ideal instrument ILS. In this paper X_{CO2} is retrieved from EM27/SUN observations with the GGG2014 retrieval algorithm (Wunch et al., 2015), which assumes the ideal ILS. However, modulation efficiency (ME) and phase error (PE) are two parameters from LINEFIT retrievals of the ILS that can be used as an indication of instrument performance and stability over time. Modulation efficiency is the ratio of the normalized modulation of the actual FTS (non-ideal ILS) and the normalized modulation of the ideal instrument ILS as function of optical path difference (OPD), so the ideal ILS will have a ME of unity (Hase, 2012). Deviations from unity in ME are a result of attenuation in the signal as a function of OPD (Wunch et al., 2007). The phase error is the angle between the real and imaginary parts of the Fourier Transform of the ILS and nonzero PE reflects asymmetry in the ILS (Wunch et al., 2007). Following Hedelius et al. (2016), Table S1 reports single ME and PE values at the maximum OPD (MOPD) (Frey et al., 2015) for each ILS measurement collected since the start of observations in Fairbanks in 2016. All results for ME and PE in Table S1 are approximately the same or better than those reported by Hedelius et al. (2016) or Frey et al. (2019). In addition, note that the KIT EM27/SUN shows a remarkable decrease in PE in 2019 relative to ILS measurements collected before the detector upgrade in 2018.

Table S1. Results from Instrument Line Shape tests for KIT and LANL EM27/SUNs.

Date	KIT EM27/SUN ME/AU, PE/mrad	LANL EM27/SUN ME/AU, PE/mrad
5 August 2016	0.9910, 2.155	0.9857, -1.395
17 March 2017	0.9839, 2.308	–
16 November 2017	0.9848, 2.281	–
9 December 2017	–	0.9993, -2.128
27 September 2018	–	0.9964, 2.635
4 October 2018	–	0.9943, 2.727
21 January 2019	0.9853, 0.3386	–

1.2 EM27/SUN bias correction to TCCON

The LANL EM27/SUN was used as a transfer standard to rescale EM27/Sun retrievals to the TCCON trace-gas scale using side-by-side comparisons with the Caltech TCCON in Pasadena. Fairbanks observations used in this paper for August 2016 through October 2017 were collected by the LANL EM27, and there are two correlations between the LANL EM27 and the Caltech TCCON instrument both before and after this data collection period. These observations (2016-2017) were bias corrected to TCCON using a linear interpolation between the multiplicative offset observed by Hedelius et al. (2016) in January 2015,

$$\text{TCCON} = \frac{1}{1.0006} \times \text{LANL},$$

and the multiplicative offset observed in December 2017, shown in Fig. S1 panel (c),

$$\text{TCCON} = \frac{1}{0.9966} \times \text{LANL},$$

as a function of days since 1 January 2015. The daily BC value was applied to all LANL EM27 observations as follows:

$$\text{LANL}_{corrected} = BC \times \text{LANL}. \quad (1)$$

Because the KIT EM27 was the instrument observing continuously at UAF in 2018 and side-by-side observations between the KIT EM27 and LANL EM27 showed that these instruments maintained a stable relationship through the summer months in 2018, only one constant bias correction term was applied to EM27/SUN retrievals of X_{CO2} collected in Fairbanks in 2018. The 2018 bias correction was determined to be the ratio of the slope of LANL EM27 vs. KIT EM27 (Fig. S1 panel (b)) and the slope of LANL EM27 vs. Caltech TCCON (Fig. S1 panel (d)) such that

$$\text{TCCON} = \frac{1.0001}{0.9991}\text{KIT}.$$

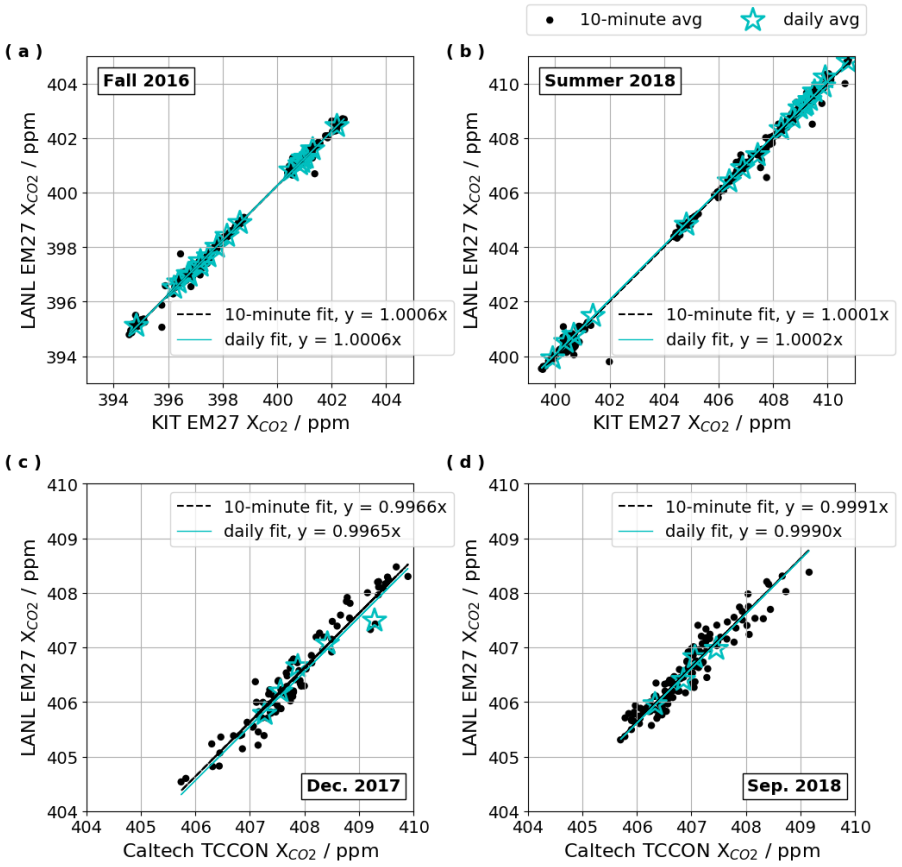

Figure S1. Correlations between LANL EM27/SUN and KIT EM27/SUN in side-by-side observations in Fairbanks (a and b), and between LANL EM27/SUN and Caltech TCCON in Pasadena (c and d).

2 Averaging kernel correction derivation

Following the methods discussed by Rodgers and Connor (2003), the difference between the retrieved, $\mathbf{x}_{ri}$, and a priori profile, $\mathbf{x}_{ai}$, for instrument i can be described as the difference between the true profile, $\mathbf{x}_T$, and a priori profile, scaled by the averaging kernel matrix of instrument i, $\mathbf{A}_i$, such that

$$\mathbf{x}_{ri} - \mathbf{x}_{ai} = \mathbf{A}_i \left(\mathbf{x}_T - \mathbf{x}_{ai}\right). \tag{2}$$

The pressure weighting function, $\mathbf{h}^T$, is described by Connor et al. (2008) and Wunch et al. (2011), and represents the pressure thickness of dry air in each layer of the profile. The dry air mole fraction of CO_2 is obtained by applying the pressure weighting function to the CO_2 profile, so

$$X_{CO2} = \frac{\text{column } CO_2}{\text{column dry air}} = \mathbf{h}^T \mathbf{x}. \tag{3}$$

From here, we define $c_{ri} = h^T \mathbf{x}_{ri}$ as the retrieved X_{CO2} and $c_{ai} = h^T \mathbf{x}_{ai}$ as the a priori X_{CO2}. Then applying $\mathbf{h}^T$ to both sides of Eq. 2 yields

$$c_{ri} = c_{ai} + \mathbf{h}^T \mathbf{A}_i \left(\mathbf{x}_T - \mathbf{x}_{ai}\right). \tag{4}$$

Now, assign OCO-2 as instrument $i = 0$ and the ground-based instrument as $i = 1$, and suppose that the true profile is some scaling of the a priori profile such that $\mathbf{x}_T = \gamma \mathbf{x}_a$. Furthermore, we assume the ground-based retrieval to be derived from the true profile, $c_{r1} = \mathbf{h}^T \gamma \mathbf{x}_{a1}$. Therefore, given a normalized column averaging kernel for instrument i, defined by Connor et al. (2008) as

$$a_{i,j} = \left(\mathbf{h}^T \mathbf{A}_i\right)_j \frac{1}{h_j}, \tag{5}$$

Eq. 4 can be written as

$$c_{r0} = c_{a0} + (\gamma - 1) \sum_j h_j (a_0)_j (x_a)_j \tag{6}$$

where $\gamma = \dfrac{c_{r1}}{c_{a1}}$. Because OCO-2 ACOS retrievals and GGG2014 use the same a priori profiles,

$$c_{r1} - \frac{c_{r1}}{c_{a1}} c_{a0} = 0,$$

and adding this to the right side of Eq. 6 yields

$$c_{r0} = c_{r1} + \left(1 - \frac{c_{r1}}{c_{a1}}\right) \sum_j h_j \left(1 - (a_0)_j\right) (x_a)_j. \tag{7}$$

Hence Eq. 7 can be used to simulate an OCO-2 retrieval of X_{CO2} that would result from assuming that the ground-based retrieval is "truth" and rescaling with the OCO-2 averaging kernel. In practice, we define an averaging kernel correction factor for each coincident OCO-2 retrieval,

$$d\text{NNG} = \left(1 - \frac{c_{r1}}{c_{a1}}\right) \sum_j h_j \left(1 - (a_0)_j\right) (x_a)_j, \tag{8}$$

using the CO_2 a priori profiles, pressure weighting functions, and averaging kernel vectors reported in the OCO-2 Lite files (OCO-2 Science Team/Michael Gunson, Annmarie Eldering, 2018). When the averaging kernel correction factor is applied to ground-based near noon aggregation, the result is a set of averaging kernel corrected ground-based observations that each correspond to a single coincident sounding, which we assign the following notation:

$$\tilde{X}_{\text{NNG}} = X_{\text{NNG}} + d\text{NNG} \tag{9}$$

where the NNG X_{CO2} retrieval aggregate (explained further in the manuscript) is defined as X_{NNG}.

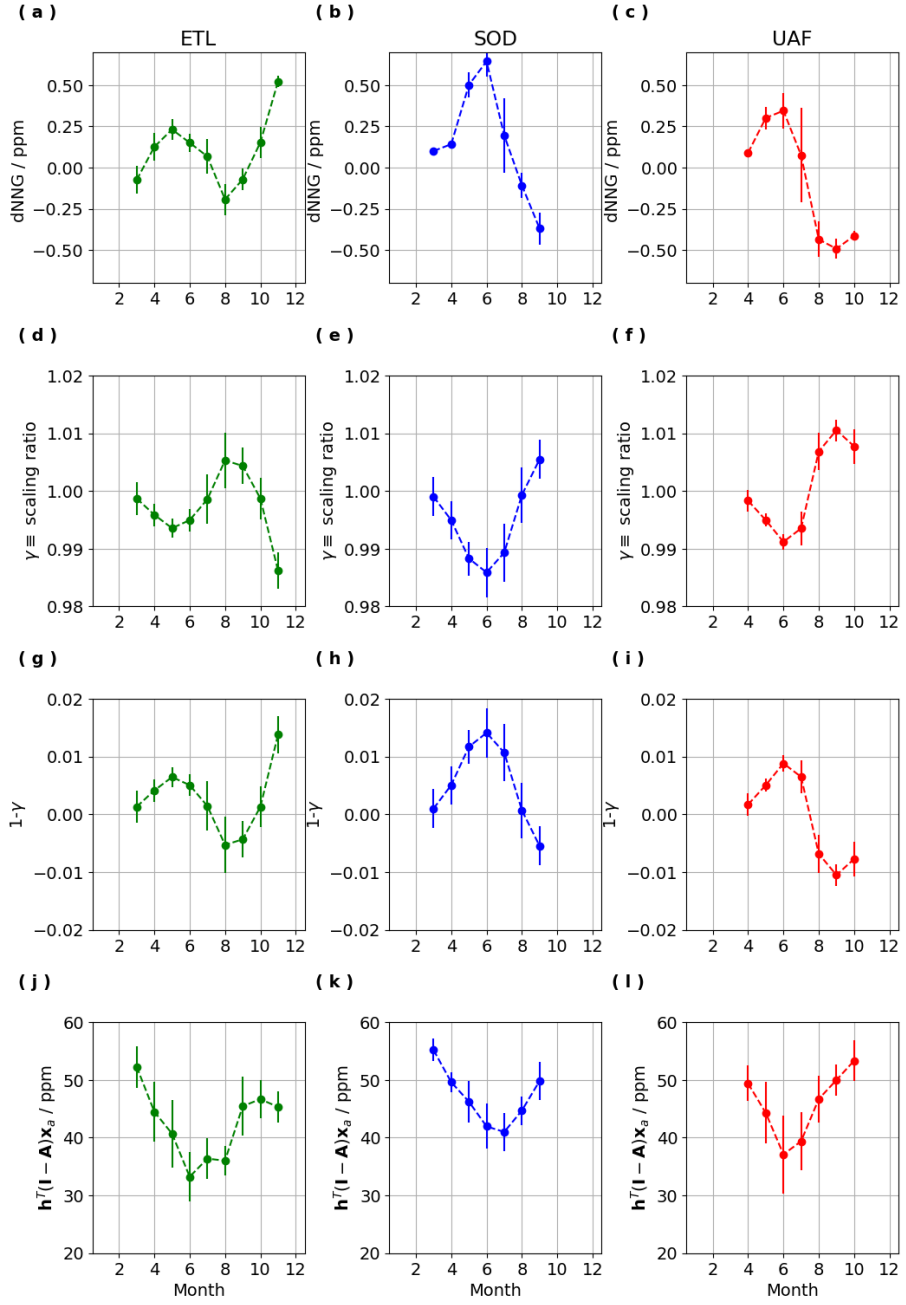

Figure S2. Monthly averages of the averaging kernel correction terms *d*NNG, and the terms composing *d*NNG, which includes the ratio of retrieved to a priori ground-based X_{CO2} ($\gamma \equiv$ scaling ratio), the modified scaling ratio ($1-\gamma$), and the averaging kernel adjusted a priori dry air mole fraction of CO_2 from OCO-2. Note that "ETL" refers to East Trout Lake, "SOD" refers to Sodankylä, and "UAF" refers to Fairbanks.

Table S2. Descriptions of OCO-2 parameters used for QC filters in B8 QC, B9 QC, and Boreal QC or otherwise discussed in the manuscript (Osterman et al., 2018; Kiel et al., 2019).

Name	Units	Description
co2_ratio	–	Ratio of single-band X_{CO2} retrieved by the 2.06 μm band to the 1.61 μm band, with the IMAP-DOAS algorithm.
h2o_ratio	–	Ratio of single-band X_{H2O} retrieved by the 2.06 μm band to the 1.61 μm band, with the IMAP-DOAS algorithm.
altitude_stddev	m	Standard deviation in surface elevation in the sounding field of view.
max_declocking_wco2	%	An estimate of the absolute value of the clocking error in the 1.61 μm band.
dpfrac	ppm	$X_{CO2,raw}\left(1-\frac{\text{a priori surface pressure in the strong CO}_2\text{ band}}{\text{retrieved surface pressure}}\right)$ where $X_{CO2,raw}$ is retrieved X_{CO2} without the B9 bias correction.
dp	hPa	The difference between the retrieved and a priori surface pressure from GEOS5-FP-IT.
dp_o2a	hPa	The difference between retrieved and a priori surface pressure at the pointing location of the O_2 A band.
dp_sco2	hPa	The difference between retrieved and a priori surface pressure at the pointing location of the strong CO_2 band.
dp_abp	hPa	Difference between retrieved and a priori surface pressure from the fast O_2 A band only preprocessor.
co2_grad_del	ppm	Difference in CO_2 vertical gradient (surface minus level 13) between retrieved and a priori profiles.
albedo_sco2	–	Retrieved 2.06 μm band reflectance.
rms_rel_wco2	%	Residual mean squared of the 1.61 μm band relative to the continuum signal.
rms_rel_sco2	%	Residual mean squared of the 2.06 μm band relative to the continuum signal.
s31	–	Ratio of signal in the 2.06 μm band to the 0.76 μm band.
albedo_slope_sco2	–	Retrieved 2.06 μm band reflectance slope.
aod_total	–	Sum of retrieved extinction optical depths of all cloud and aerosols at 0.755 μm.
dws	–	Sum of retrieved extinction optical depths of dust, water, and seasalt at 0.755 μm.
aod_water	–	Retrieved extinction optical depth of cloud water at 0.755 μm.
aod_ice	–	Retrieved extinction optical depth of cloud ice at 0.755 μm.
ice_height	–	Retrieved ice cloud height as a ratio of atmospheric pressure to retrieved surface pressure.
aod_sulfate + aod_oc	–	Sum of retrieved extinction optical depths of sulfate and organic carbon aerosols at 0.755 μm.
aod_strataer	–	Retrieved extinction optical depth of total aerosols in the upper troposphere and stratosphere at 0.755 μm.
aod_oc	–	Retrieved extinction optical depth of organic carbon aerosols at 0.755 μm.
aod_seasalt	–	Retrieved extinction optical depth of seasalt aerosols at 0.755 μm.
deltaT	K	Retrieved offset to the a priori temperature profile.
sza	degrees	Solar zenith angle (with 90° at the horizon and 0° directly overhead).
xco2_uncertainty	ppm	Retrieval error in X_{CO2}.
tcwv	kg m^{-2}	Retrieved total column water vapor obtained by multiplying retrieved scaling factor by prior from the ECMWF (European Centre for Medium-Range Weather Forecasts).

References

Butz, A., Dinger, A. S., Bobrowski, N., Kostinek, J., Fieber, L., Fischerkeller, C., Giuffrida, G. B., Hase, F., Klappenbach, F., Kuhn, J., Lübcke, P., Tirpitz, L., and Tu, Q.: Remote sensing of volcanic CO_2, HF, HCl, SO_2 and BrO in the downwind plume of Mt. Etna, Atmos. Meas. Tech., 10, 1–14, https://doi.org/10.5194/amt-10-1-2017, www.atmos-meas-tech.net/10/1/2017/doi:10.5194/amt-10-1-2017, 2017.

Connor, B. J., Boesch, H., Toon, G. C., Sen, B., Miller, C., and Crisp, D.: Orbiting Carbon Observatory: Inverse method and prospective error analysis, J. Geophys. Res., 113, https://doi.org/10.1029/2006JD008336., 2008.

Frey, M., Hase, F., Blumenstock, T., Groß, J., Kiel, M., Mengistu Tsidu, G., Schäfer, K., Sha, M. K., and Orphal, J.: Calibration and instrumental line shape characterization of a set of portable FTIR spectrometers for detecting greenhouse gas emissions, Atmos. Meas. Tech., 8, 3047–3057, https://doi.org/10.5194/amt-8-3047-2015, 2015.

Frey, M., Sha, M. K., Hase, F., Kiel, M., Blumenstock, T., Harig, R., Surawicz, G., Deutscher, N. M., Shiomi, K., Franklin, J. E., Bösch, H., Chen, J., Grutter, M., Ohyama, H., Sun, Y., Butz, A., Mengistu Tsidu, G., Ene, D., Wunch, D., Cao, Z., Garcia, O., Ramonet, M., Vogel, F., and Orphal, J.: Building the COllaborative Carbon Column Observing Network (COCCON): long-term stability and ensemble performance of the EM27/SUN Fourier transform spectrometer, Atmos. Meas. Tech., 12, 1513–1530, https://doi.org/10.5194/amt-12-1513-2019, 2019.

Hase, F.: Improved instrumental line shape monitoring for the ground-based, high-resolution FTIR spectrometers of the Network for the Detection of Atmospheric Composition Change, Atmos. Meas. Tech., 5, 603–610, https://doi.org/10.5194/amt-5-603-2012, 2012.

Hase, F., Blumenstock, T., and Paton-Walsh, C.: Analysis of the instrumental line shape of high-resolution Fourier transform IR spectrometers with gas cell measurements and new retrieval software, Appl. Optics, 38, 3417–3422, https://doi.org/10.1364/AO.38.003417, 1999.

Hase, F., Hannigan, J. W., Co1ey, M. T., Goldman, A., Höpfner, M., Jones, N. B., Rinsland, C. P., and Wood, S. W.: Intercomparison of retrieval codes used for the analysis of high-resolution, ground-based FTIR measurements, J. Quant. Spectrosc. Ra., 87, 25–52, https://doi.org/10.1016/j.jqsrt.2003.12.008, 2004.

Hase, F., Frey, M., Kiel, M., Blumenstock, T., R., H., Keens, A., and Orphal, J.: Addition of a channel for XCO observations to a portable FTIR spectrometer for greenhouse gas measurements, Atmos. Meas. Tech., 9, 2303 – 2313, https://doi.org/10.5194/amt-9-2303-2016, 2016.

Hedelius, J. K., Viatte, C., Wunch, D., Roehl, C. M., Toon, G. C., Chen, J., Jones, T., Wofsy, S. C., Franklin, J. E., Parker, H., Dubey, M. K., and Wennberg, P. O.: Assessment of errors and biases in retrievals of X_{CO2}, X_{CH4}, X_{CO}, and X_{N2O} from a 0.5 cm^{-1} resolution solar-viewing spectrometer, Atmos. Meas. Tech., 9, 3527–3546, https://doi.org/10.5194/amt-9-3527-2016, 201, 2016.

Kiel, M., O'Dell, C. W., Fisher, B., Eldering, A., Nassar, R., MacDonald, C. G., and Wennberg, P. O.: How bias correction goes wrong: measurement of X_{CO2} affected by erroneous surface pressure estimates, Atmos. Meas. Tech., 12, 2241–2259, https://doi.org/10.5194/amt-12-2241-2019, https://doi.org/10.5194/amt-12-2241-2019, 2019.

OCO-2 Science Team/Michael Gunson, Annmarie Eldering: OCO-2 Level 2 bias-corrected XCO2 and other select fields from the full-physics retrieval aggregated as daily files, Retrospective processing V9r, Greenbelt, MD, USA, Goddard Earth Sciences Data and Information Services Center (GES DISC), https://doi.org/10.5067/W8QGIYNKS3JC, https://disc.gsfc.nasa.gov/datasets/OCO2_L2_Lite_FP_9r/summary, Accessed: [18 December 2018], 2018.

Osterman, G. B., Eldering, A., Avis, C., Chafin, B., O'Dell, C., Frankenberg, C., Fisher, B., Mandrake, L., Wunch, D., Granat, R., and Crisp, D.: Data Product User's Guide, Operational L1 and L2 Data Versions 8 and Lite File Version 9, https://docserver.gesdisc.eosdis.nasa.gov/public/project/OCO/OCO2_DUG.V9.pdf, 2018.

Rodgers, C. D. and Connor, B. J.: Intercomparison of remote sounding instruments, J. Geophys. Res., 108, 4116, https://doi.org/doi:10.1029/2002JD002299, 2003.

Wennberg, P. O., Wunch, D., Roehl, C. M., Blavier, J.-F., Toon, G. C., and Allen, N. T.: TCCON data from Caltech (US), Release GGG2014.R1 TCCON data archive, hosted by CaltechDATA, California Institute of Technology, Pasadena, CA, U.S.A., https://doi.org/10.14291/tccon.ggg2014.pasadena01.r1/1182415, 2017.

Wunch, D., Taylor, J. R., Fu, D., Bernath, P., Drummond, J. R., Midwinter, C., Strong, K., and Walker, K. A.: Simultaneous ground-based observations of O_3 , HCl, N_2O, and CH_4 over Toronto, Canada by three Fourier transform spectrometers with different resolutions, Atmos. Chem. Phys., 7, 1275–1292, www.atmos-chem-phys.net/7/1275/2007/, 2007.

Wunch, D., Wennberg, P. O., Toon, G. C., Connor, B. J., Fisher, B., Osterman, G. B., Frankenberg, C., Mandrake, L., O'Dell, C., Ahonen, P., Biraud, S. C., Castano, R., Cressie, N., Crisp, D., Deutscher, N. M., Eldering, A., Fisher, M. L., Griffith, D. W. T., Gunson, M., Heikkinen, P., Keppel-Aleks, G., Kyro, E., Lindenmaier, R., Macatangay, R., Mendonca, J., Messerschmidt, J., Miller, C. E., Morino, I., Notholt, J., A, F., Oyafuso, Rettinger, M., Robinson, J., Roehl, C. M., Salawitch, R. J., Sherlock, V., Strong, K., Sussmann, R., Tanaka, T., Thompson, D. R., Uchino, O., Warneke, T., and Wofsy, S. C.: A method for evaluating bias in global measurements of CO_2 total columns from space, Atmos. Chem. Phys., 11, 12 317–12 337, https://doi.org/10.5194/acp-11-12317-2011, www.atmos-chem-phys.net/11/12317/2011/ Atmospheric, 2011.

Wunch, D., Toon, G. C., Sherlock, V., Deutscher, N. M., Liu, C., Feist, D. G., and Wennberg, P. O.: The Total Carbon Column Observing Network's GGG2014 Data Version, 43, https://doi.org/10.14291/tccon.ggg2014.documentation.R0/1221662, http://tccon.ornl.gov, 2015.